Epigenetic silencing of IRF1 dysregulates type III interferon responses to respiratory virus infection in epithelial to mesenchymal transition

Jun Yang[1,2], **Bing Tian**[1,2], **Hong Sun**[1], **Roberto P. Garofalo**[2,4], and **Allan R. Brasier**[1,2,3,*]

[1]Department of Internal Medicine, University of Texas Medical Branch, Galveston, TX 77555

[2]Department of Sealy Center for Molecular Medicine, University of Texas Medical Branch, Galveston, TX 77555

[3]Institute for Translational Sciences, University of Texas Medical Branch, Galveston, TX 77555

[4]Department of Pediatrics, University of Texas Medical Branch, Galveston, TX 77555

Abstract

Chronic oxidative injury produced by airway disease triggers TGFβ-mediated epigenetic reprogramming known as the epithelial-mesenchymal transition (EMT). We observe that EMT silences protective mucosal interferon (IFN)-I/-III production associated with enhanced rhinovirus (RV) and respiratory syncytial virus(RSV) replication. Mesenchymal transitioned cells are defective in inducible interferon regulatory factor (IRF)1 expression by occluding RelA and IRF3 access to the promoter. IRF1 is necessary for expression of type III IFNs (IFNLs-1 and 2/3). Induced by the EMT, Zinc Finger E-Box Binding Homeobox 1 (ZEB1) binds and silences *IRF1*. Ectopic ZEB1 is sufficient for *IRF1* silencing, whereas ZEB1 knockdown partially restores *IRF1-IFNL* upregulation. ZEB1 silences *IRF1* through the catalytic activity of the Enhancer of Zeste 2 Polycomb Repressive Complex 2 Subunit (EZH2), forming repressive H3K27(me3) marks. We observe that *IRF1* expression is mediated by ZEB1 de-repression; our study demonstrates how airway remodeling/fibrosis is associated with a defective mucosal antiviral response through ZEB1-initiated epigenetic silencing.

*Corresponding author: Allan R. Brasier, MD, MRB 8.126, University of Texas Medical Branch, 301 University Blvd, Galveston, TX 77555-1060, Phone: 409-772-8705, FAX 409-772-8709, arbrasie@utmb.edu. Correspondence and requests for materials should be addressed to J.Y. (junyang@utmb.edu) and A.R.B. (arbrasie@utmb.edu).

Introduction

The airway mucosal barrier plays a central role in the pathogenesis of reactive airway disease (asthma), a major public health concern affecting ~ 4% of the population worldwide [1]. Asthma involves chronic oxidative damage-induced epithelial cell injury and barrier dysfunction [2]. Chronic epithelial injury activates the transforming growth factor (TGFβ) pathway to promote mucosal repair [3]. TGFβ signaling induces airway remodeling, a permanent structural change characterized by subepithelial fibrosis and myofibroblast expansion [3]. Subepithelial collagen deposition is an early event, preceding Th2 cell polarization and eosinophil accumulation [4]. Consequently remodeling may play an etiological role in reactive airways disease.

The epithelial barrier also plays a major role in the episodic decompensations commonly triggered by viral respiratory tract infections [5], particularly respiratory syncytial virus (RSV) in infants and rhinovirus (RV) in children and adults [6, 7]. RSV and RV replicate in the airway epithelium, triggering an innate inflammatory response. Pathogen-associated molecular patterns (PAMPs) produced by RV and RSV replication are recognized by the membrane-anchored pattern recognition receptor (PRR) TLR3 and the cytoplasmic PRRs, RIG-I and MDA5 [8, 9], to trigger cascades of interferon regulatory factor (IRF) responses. The IRF cascade is initially triggered by constitutively expressed IRF3, whose activation induces expression of IRF1 and −7 in epithelial cells. IRF-1/7 amplify expression of the RIG-I pattern recognition receptor[10] and of protective type I IFNs (IFN α/β) [11]. Type I IFNs trigger the intracellular Jak-STAT pathway controlling ~300 IFN-stimulated genes (ISGs) that inhibit viral replication, activate innate lymphocytes and stimulate leukocyte recruitment [12]. Viral PAMPs also activate epithelial IFN-III (IFNLs) expression by incompletely understood mechanisms [9, 13]. In contrast to IFN-I, IFN-III binds to an epithelial-restricted class II cytokine receptor converging on Jak-STAT activation and ISG expression. Consequently, IFN-III plays a role in innate immunity to mucosal pathogens, including RV [14, 15].

Severe asthmatics are susceptible to sino-pulmonary infections [16]. Undoubtedly, the etiology for this impaired mucosal innate immunity is multifactorial; reduced production of IFN-III [17] has been related to exacerbation severity [18]. One study reported that RV replicates more efficiently in asthmatic epithelium associated with defective IFN-III production [19]. The relationship between airway remodeling and defective innate immunity has not been systematically established [20, 21, 22]. Here, we examine the mechanism for enhanced viral replication in epithelial cells subjected to mesenchymal reprogramming and implicate a role for epigenetic silencing of the IRF1 pathway via the EZH2 histone methyltransferase activity.

Results

Mesenchymal transition silences the epithelial IFN-III response

We examined TLR3 and RIG-I antiviral signaling in a standardized model of mesenchymal reprogramming using primary human small airway epithelial cells (hSAECs)[23]. TGFβ treatment of hSAECs triggers the characteristic genomic [24, 25] and proteomic [26] signatures

of the mesenchymal state. The EMT is accompanied by coordinate repositioning of activating and repressing histone epigenetic marks – H3K4Ac and H3K27me3, respectively – on the enhancers of ~ 3 K genes in the TGFβ network [24, 27]. To illustrate, control and TGFβ-treated hSAECs were analyzed by confocal microscopy. Here, untreated controls showed peripheral cytoplasmic distribution of polymeric actin, while TGFβ-treated hSAECs (EMT-hSAECs) showed a marked enhancement of organized mesenchymal stress fibers throughout the cytoplasm. Loss of the epithelial marker E-cadherin (CDH1) and acquisition of mesenchymal marker vimentin (VIM) further illustrates that the TGFβ-treated hSAECs have undergone EMT (Fig. 1a).

Experiments comparing IFN secretion patterns in the epithelial vs mesenchymal state were first conducted after activating Toll-like receptor (TLR3) signaling using extracellular poly(I:C). *IFNA1* mRNA expression showed a 4-fold induction, peaking after 6 h in control hSAECs; EMT-hSAECs had a slightly more rapid response, peaking after 4 h of stimulation (Fig. 1b). By contrast, expression of *IFNB1* was dramatically affected; in the control cells, we observed an 11-fold induction of *IFNB1* mRNA by 4 h of poly(I:C) stimulation, whereas <3-fold induction was produced in the EMT-hSAECs (p<0.05; Fig. 1c). An even more marked inhibition of IFN-III expression was observed in EMT-hSAECs. The 2,100-fold increased expression of *IFNL1 (IL-29)* in control hSAECs was less than 40-fold in EMT-hSAECs, and the 450-fold expression of *IFNL2/3* (*IL-28A/B*) was similarly attenuated (Fig. 1d,e).

To determine whether these changes functionally reduced downstream ISG expression, we measured the expression of MX Dynamin-Like GTPase 1 (*MX1*) and Retinoic acid inducible gene-I (*RIG-I*). *MX1* was highly induced, by 79-fold in hSAECs but by less than 2-fold in EMT-hSAECs after 4 h of poly(I:C) stimulation (Fig. 1f). Similar results were observed for the 400-fold induction of *RIG-I* in hSAECs *vs* <10-fold in EMT-hSAECs (Fig. 1g). These data indicate that IFN-I and III expression and the downstream ISG response were attenuated by mesenchymal transition.

We next explored the differential responses to RNA viruses associated with exacerbations of reactive airway disease, including RSV and RV. Both viruses trigger innate inflammation via RIG-I [8, 9]. Similar attenuation of *MX1* (Fig. 1h) and *RIG-I* (Fig. 1i) expression were observed after RV infection in EMT-hSAECs. We noted enhanced release of RSV virions at 12- and 24 h post infection (p.i.) in EMT-hSAECs (Fig. 1j). A more striking enhancement of RV replication was observed in EMT-hSAECs, with a greater than 3-log increase in pfu at 12 and 24 h (Fig. 1k). Images of the plaque assays are shown in Fig. 1l and Supplementary Figure 1. These data demonstrate that the defects in IFN-I/III - ISG pathway in the EMT-hSAECs were functionally important.

Mesenchymal transition silences IRF1 expression by promoter occlusion

We further explored the mechanism for defective IFN-I/III production in EMT-hSAECs. We focused on the IRFs, since the inducible IRF1 and −7 proteins play a major role in type I IFN expression, by amplifying RIG-I expression. *IRF1* mRNA was induced 13-fold after 4 h of poly(I:C) stimulation in hSAECs, but its basal and poly(I:C)-induced activities were completely blocked in EMT-hSAECs (p<0.05, all conditions, Fig. 2a). By contrast, *IRF7*

expression was slightly enhanced in EMT-hSAECs (Fig. 2b), while *IRF3* expression was not affected (Supplementary Figure 2). This differential IRF1 expression was evident by Western (Fig. 2c). To confirm defective IRF1 induction, we measured IRF1 DNA-binding activity by a quantitative microaffinity binding assay [28] using a high-affinity ISG duplex from the *IFNB1* promoter [29]. We observed strong induction of IRF1 DNA binding in hSAECs, which was significantly decreased in EMT-hSAECs (Fig. 2d). The effect of mesenchymal transition on defective IRF1 expression was analyzed by immunofluorescence staining. In the absence of stimulation, no IRF1 staining was detected; however, poly(I:C) induced strong IRF1 nuclear accumulation in hSAECs (Fig. 2e, top). By contrast, IRF1 staining in EMT-hSAECs was significantly lower, irrespective of poly(I:C) stimulation (Fig. 2e, bottom; also note the dramatic mesenchymal phenotype by phalloidin staining).

In epithelial cells, IRF1 is induced through combinatorial actions of NFκB and IRF3. To understand how the mesenchymal state interferes with IRF1 expression, we performed a two-step chromatin-immunoprecipitation (XChIP) assay [30]. Using XChIP, we quantitated NFκB/RelA and IRF3 binding to the *IRF1* promoter in hSAECs stimulated with poly(I:C), or infected with RSV, vs that in EMT-hSAECs. Basal binding of IRF3 and RelA was decreased in EMT-hSAECs (Fig. 2f). This difference was even more apparent in response to poly(I:C) and RSV infection, where IRF3 and RelA binding was largely induced in hSAECs, but dramatically blocked in EMT-hSAECs (Fig. 2f). Because IRF3 and RelA expression is unaffected by EMT[31], these data indicate to us that the chromatin environment of *IRF1* in the mesenchymal state is not permissive for viral inducible transcription factor binding.

We next determined whether the decrease in IRF1 expression/translocation was sufficient to reduce binding to the endogenous *IFNB1* promoter; we measured IRF1 binding to *IFNB1* by XChIP[30]. Poly(I:C) induced an 11-fold increase in IRF1 binding to *IFNB1* relative to control treatment in hSAECs; this was reduced to <5-fold in EMT-hSAECs (Fig. 2g, left panel). IRF1 mediates IFNL expression downstream of ROS generation by the peroxisome [32]. Analysis of the *IFNL1* promoter also showed a highly inducible, 38-fold increase in IRF1 binding in poly(I:C)-stimulated hSAECs that was reduced to ~13-fold in EMT-hSAECs (Fig. 2g, right panel). Binding of IRF7 to endogenous *IFNB1* and *IFNL1* showed a similar 2.8-fold induction in XChIP (Fig. 2h). Interestingly, despite the increase in IRF7 expression with mesenchymal transition (Fig. 2c), IRF7 binding to the endogenous *IFNB1* and *IFNL1* promoters was greatly reduced in EMT-hSAECs. We excluded the unlikely possibility that enhanced IRF7 expression is somehow responsible for silencing *IFNB1*/*IFNL1* expression by coactivator competition in trans by conducting an IRF7 knockdown experiment in EMT-hSAECs (Supplementary Figure 3). IRF7 depletion slightly inhibited poly(I:C)-induced *MX1* induction (Fig. 2i), and had no effect on *RIG-I* induction (Fig. 2j). Collectively, these data indicate that the mesenchymal transition is associated with decreased IRF1 expression due to promoter inaccessibility.

Modulation of IRF1 expression reverses type I/III IFN expression and restores antiviral immunity

Viral pattern-inducible IFN expression is controlled by transcription factor complexes of the NFκB, IRF and AP-1 families [33]. To determine whether IRF1 is necessary for IFN-I/III expression in the mesenchymal background, we performed a time-course of poly(I:C) stimulation of EMT-hSAECs complemented with ectopic IRF1 (Supplementary Figure 4). IRF1 transfectants induced significantly more *IFNB1* and *IFNL1* mRNAs than in empty vector controls (Fig. 2k,l). In the same transfectants infected with RV, *IFNB1* and *IFNL1* mRNAs were significantly induced (Supplementary Figure 5), and RV titers were significantly reduced at 8 and 24 h p.i. in the IRF1-transfectants (Fig. 2m). These data indicate that IRF1 expression is limiting for maximal IFN-I and -III responses and the restriction of viral replication.

To determine whether IRF1 expression is required for IFN-I/III production in normal hSAECs (non-EMT background), we silenced IRF1 expression using genome editing. Stable transfectants were isolated and effects on poly(I:C)-inducible IRF1 expression determined by Western blot. Poly(I:C) induced high IRF1 expression in control transfectants; IRF1 expression was completely abolished in those subjected to CRISPR/Cas 9 genome editing (Fig. 3a). We noted that the rapid induction of *IFNB1* 2 h after poly(I:C) activation was completely lost in the IRF1-deficient hSAECs, although 4 h later *IFNB1* expression was induced via a compensatory mechanism (Fig. 3b). The induction of *IFNL1* was more dramatically affected in the IRF1-deficient hSAECs at all time points (Fig. 3c). RV infection in IRF1-deficient hSAECs showed that CRISPR/Cas 9-mediated IRF1 knockout decreased the induction of *IFNB1* (Fig. 3d) and *IFNL1* (Fig. 3e) and increased RV virus replication (Fig. 3f). Collectively, these studies indicate that IRF1 is rate-limiting for maximal IFN-I and III expression and the restriction of RV infection.

The core EMT regulator Zinc Finger E-Box Binding Homeobox 1 (ZEB1) silences IFN-I and -III expression

The mesenchymal transition is a multi-step cell state change driven by a double-negative ZEB1-SNAI feedback loop with miRNAs [34]. In hSAECs, the TGFβ-induced mesenchymal transition induces robust activation of *SNAI1*, *ZEB1/2*, and to a lesser extent, *Twist1* at the mRNA levels (Fig. 4a). Because ZEB1 has been shown to regulate IFN-III gene expression [35] and earlier ChIP-Seq studies showed major peaks of ZEB1/2 binding to the *IRF1* promoter (Supplementary Figure 8), we focused first on identifying which ZEB isoform plays a functional role in IRF1 regulation during the mesenchymal transition. Although ZEB2 is the most highly expressed ZEB isoform in EMT-hSAECs, it only weakly binds *IRF1* (Supplementary Figure 6), leading us to explore the functional role of ZEB1. From a low basal expression of ZEB1 in epithelial cells, a significant upregulation was observed in EMT-hSAECs by Western blot (Fig. 4b) and immunofluorescence microscopy (Fig. 4c). To establish physiological relevance, we used immunofluorescence microscopy to examine whether ZEB1 is upregulated in an established mouse model of airway fibrosis. Here, chronic TGFβ stimulation induced ZEB1 expression uniformly in the airway epithelium (Fig. 4d).

We next determined whether ZEB1 expression is required for IFN silencing in hSAECs. hSAECs transduced with lentiviral *ZEB1* cDNA showed significant upregulation of ZEB1 protein by Western blot (Fig. 4e), as well as spindle-shaped morphological changes, consistent with its actions on cytoskeletal remodeling [36] (Supplementary Figure 9). Control or ZEB1-expressing hSAECs were then stimulated with poly(I:C) and the time course of IFN-I/III expression examined. We found that both *IFNB1* and *IFNL1* mRNA induction was significantly decreased in ZEB1-expressing transfectants relative to controls (Fig. 4f,g). In response to RV16 infection, *IFNL-1* and *-2/3* mRNAs were also significantly decreased in ZEB1-expressing transfectants (Fig. 4h,i). Consistently, RV16 also replicated more efficiently in the ZEB1 transfectants, releasing a 2.5-fold higher titer of infectious virions 24 h p.i. (Fig. 4j). These data indicate that ZEB1 is sufficient for silencing IFN-I and -III expression in response to viral PAMPs.

ZEB1 silencing restores mucosal IFN production in EMT-hSAECs

Although ZEB1 expression in the differentiated hSAECs suppressed mucosal IFN production, we next asked whether ZEB1 expression is required in the mesenchymal background. For this purpose, we evaluated the silencing effect of three doxycycline (Dox)-inducible lentiviral shRNAs specific for *ZEB1*. All three significantly reduced *ZEB1* expression; shRNA1 was slightly more effective by Q-RT-PCR (Supplementary Figure 10) and Western immunoblot (Fig. 4k). hSAECs were transitioned into the mesenchymal state by tonic TGFβ stimulation in Dox-free medium. ZEB1 was then silenced by Dox administration prior to a time course of poly(I:C) challenge. Remarkably, the ZEB1-depleted cells showed a much stronger induction of *IFNB1* (Fig. 4l) and *IFNL1* (Fig. 4m) across all time points. Collectively, these data show that ZEB1 downregulates IFN I and III expression in both normal and EMT-hSAECs.

ZEB1 inhibition of mucosal IFNs is mediated by IRF1 repression

Because we observed that IRF1 was rate-limiting for mucosal IFN production, and ZEB1 has been shown to bind to the *IRF1* promoter in ChIP-seq experiments (Supplementary Figure 8), we tested whether ZEB1 represses IRF1 as its mechanism for inhibition of IFN expression. First, we asked whether inducible *IRF1* expression is restored in the EMT-hSAECs after ZEB1 silencing. EMT-hSAECs expressing *ZEB1*-targeting shRNA1 were TGFβ-transitioned, treated +/− Dox, and then stimulated with poly(I:C). We observed a 48-fold induction of *IRF1* mRNA in the ZEB1-silenced cells vs 18-fold in controls after 4 h of poly(I:C) stimulation (Fig. 5a).

The effect of ZEB1 silencing on IRF1 binding to the endogenous IFN-I/III promoters was then assayed in ZEB1-silenced cells by XChIP [30]. In the EMT-hSAECs, poly(I:C) induced weak binding of IRF1 to the *IFNB1* promoter; this induction was significantly enhanced by ZEB1 silencing (Fig. 5b, left panel). Similarly, IRF1 binding to the *IFNL1* promoter was dramatically enhanced, to 28-fold in the ZEB1 silenced cells vs 8-fold in the control cells (Fig. 5b, middle panel). A similar enhancement of IRF1 binding was observed for the *IFNL2* promoter (Fig. 5b, right panel).

A ZEB1•C-terminal binding protein CtBP•polycomb repressive complex forms repressive H3K27(me3) marks on the IRF1 promoter

Mesenchymal transition involves inhibition of epithelial genes by inducing the accumulation of repressive histone marks as a mechanism for epigenetic regulation [27]. In this regard, ZEB1 inactivates epithelial genes during the mesenchymal transition by complexing with CtBP, which functions as a molecular bridge with the polycomb repressor complex (PRC) 2, containing the EZH2 methyltransferase responsible for forming repressive histone H3 trimethylated lysine (K) 27 [H3K27(me3)] marks [37, 38]. XChIP assays were performed in the absence or presence of poly(I:C) stimulation for ZEB1, CtBP, EZH2 and activating H3K4 (me3) and repressive H3K27(me3) marks. In hSAECs, we observed that ZEB1 was associated with the *IRF1* promoter, and this association was significantly decreased by poly(I:C) stimulation (Fig. 5c, left; further evidence for specificity is in Supplementary Figure 11). Conversely, the levels of ZEB1 binding to the *IRF1* promoter were increased in EMT-hSAECs, consistent with the induction of ZEB1 by mesenchymal transition (Fig. 4a,b,c); and although poly(I:C) reduced ZEB1 binding, these levels were comparable to those of (silenced) IRF1 in control hSAECs (Fig. 5c, left).

A similar pattern of CtBP and EZH2 binding to *IRF1* was found in hSAECs and EMT-hSAECs as that observed for ZEB1 binding, consistent with the known ZEB1-CtBP-EZH2 protein-protein complex[39][37]. Analysis of the histone modifications showed that the activation-associated H3K4(me3) mark was found on the *IRF1* promoter in hSAECs and increased with poly(I:C) stimulation, consistent with *IRF1* mRNA expression (Fig. 5c, c.f. 2a). By contrast, H3K4(me3) abundance was significantly lower in both unstimulated and poly(I:C)-stimulated EMT-hSAECs relative to that in hSAECs (Fig. 5c). The repressive H3K27(me3) mark was increased on the *IRF1* promoter in control EMT-hSAECs, and although this was decreased by poly(I:C) stimulation, the levels were comparable to those on the silenced *IRF1* promoter in control hSAECs (Fig. 5c). The effect of ZEB1 silencing on CtBP and EZH2 binding and histone modifications on the *IRF1* promoter was analyzed in EMT-hSAECs by XChIP (Fig. 5d). In *ZEB1* shRNA- depleted EMT-hSAECs, the activating H3K4(me3) was increased on the *IRF1* promoter while the repressive H3K27(me3) was decreased in association with CtBP and EZH2 binding (Fig. 5d). We interpret these findings to suggest that the ZEB1-CtBP-EZH2 complex mediates mesenchymal silencing of *IRF1* by inducing the accumulation of repressive epigenetic marks. Conversely, a component of the mechanism of IRF1 induction by poly(I:C) in normal hSAECs involves promoter de-repression via decreased ZEB1-CtBP-EZH2 binding.

The association between ZEB1-CtBP-EZH2 binding and H3K27(me3) accumulation on the *IRF1* promoter prompted us to evaluate whether the EZH2 methyltransferase of the PRC2 mediates *IRF1* expression. We tested the effect of GSK126, a potent, highly selective small-molecule inhibitor of EZH2 methyltransferase activity [40]. Previous studies have shown that GSK126 decreases global H3K27(me3) levels and reactivates repressed PRC2 target genes [40]. We observed that relative to solvent-treated controls, GSK126 enhanced *IRF1* mRNA expression in EMT-hSAECs, peaking at 17-fold 96 h after addition (Fig. 5e). A similar release of inhibition of the *IFNL1* mRNA response increased 27-fold at the same time point (Fig. 5f), consistent with our earlier findings that *IRF1* expression is rate-limiting

in IFNL production. Although GSK126 produced a transient induction of *ZEB1* mRNA after 24 h, this treatment had no stable effect on *ZEB1* expression (Fig. 5g). Interestingly, GSK126 treatment enhanced the increase in *IRF1* expression by either RV16 or RSV infection in EMT-hSAECs (Fig. 5h). We also noted that GSK126 treatment slightly increased *IFNB1* production (Fig. 5i) and significantly increased *IFNL* expression for all treatments (Fig. 5j). The viral replication of both RV16 and RSV was lower as well (Fig. 5k).

Discussion

Diseases associated with chronic airway mucosal injury and repair are also associated with defects in innate immunity. This study focuses on the effects of cellular reprogramming on the expression of IFN-I/III, two major classes of paracrine mediators of the mucosal antiviral response. A major discovery in this work is that TGFβ-dependent mesenchymal transition dramatically affects the expression of IFN-IIIs, and to a lesser extent, IFNβ, through silencing of IRF1 expression. Although the virus-inducible expression of IFN-I (IFNβ) has been extensively studied, the control mechanisms for inducible IFNLs are incompletely understood. Our studies demonstrate that IRF1 is the major rate-limiting transcriptional regulator of IFNL expression, and confirm that IFNL expression plays a significant role in restricting RV replication, more so than RSV. Although the mechanisms for inducible control of *IRF1* via NFκB are well documented, little is known about its epigenetic regulation. Our studies indicate that the chromatin environment of *IRF1* is located in a metastable state in epithelial cells, with both activating histone marks (H3K4me3) and repressive marks (H3K27me3). We demonstrate that the mesenchymal transition silences *IRF1*, making the promoter inaccessible to RelA and IRF3 transactivators associated with the accumulation of repressive H3K27(me3) marks. Our data further indicate that this epigenetic silencing is mediated by ZEB1 and its PRC2 co-repressor containing the EZH2 methyltransferase. Based on these studies, we propose a unifying model for epigenetic regulation of mucosal IFNs mediated by ZEB1-PRC2 complex interaction with the *IRF1* promoter in both cell states (Fig. 6). In normal cells, in the basal state, *IRF1* is in a semi-open chromatin environment, repressed by low levels of ZEB1-CtBP interaction. In response to poly(I:C) stimulation, ZEB1-CtBP binding is cleared from the promoter, a de-repression event followed by the binding of the activators NFκB/RelA and IRF3 to mediate its dramatic upregulation [41]. Conversely, in mesenchymal transitioned cells, ZEB1-CtBP is much more abundant, and although this complex is slightly decreased upon activation of the innate pathway, this is not sufficient to clear ZEB1-CtBP or repressive H3K27(me3) marks to enable gene activation. Others shown that IRF1/type I IFN expression is developmentally controlled in embryonal stem cells, being silenced via an unknown mechanism[42]. It will be of interest to examine the role of ZEB1-PRC2 in this developmental phenomenon.

This work provides new insights into innate immune defects associated with chronic remodeling and repair. In reactive airway disease, the TGFβ pathway is activated to promote mucosal repair and renewal [3], and may also be reprogramming the mucosal IFN response. Our study provides a testable mechanism for how severe asthma is associated with defects in epithelial secretion of type III IFNs [43], and enhanced susceptibility to RV replication [19]. Similarly, mesenchymal transition is an important pathological process in idiopathic

pulmonary fibrosis and cystic fibrosis, where an upregulated TGFβ pathway and ZEB1 have been observed [44, 45]. Our findings using the GSK126 ZEB1 inhibitor suggests that the EZH2 methyltransferase may be a target for epigenetic modulation that could reverse defects in mucosal innate immunity.

Methods

Cell culture and treatment

Human small airway epithelial cells (hSAECs)[24, 46], authenticated by short tandem repeat (STR) analysis in our lab, were not listed in the database of commonly misidentified cell lines maintained by ICLAC and NCBI BioSample. hSAECs were mycoplasma free and grown as submerged monolayers in SAGM small airway epithelial cell growth medium (Lonza) with low glucose content of 1.081 g/L (6mM). To induce EMT, hSAECs were stimulated with TGFβ (10 ng/ml, PeproTech) for 15 d [24]. Poly(I:C) (Sigma-Aldrich) was solubilized in PBS and used at 50 μg/ml in cell culture. GSK126 (Selleckchem) was solubilized in DMSO as a 10mM stock and used at 10 μM for 3 d [40].

Virus preparation and infection

Respiratory syncytial virus (RSV) A2 strain was grown in HEp-2 cells (ATCC CCL-23) and prepared as previously described [11]. Rhinovirus serotype 16 (RV16, a generous gift from James E. Gern[47]) was grown in H1 HeLa cells at 35 °C as described[48]. The viral titer of RSV or RV16 was determined by standard methylcellulose plaque assay. Purified viral pools were aliquoted, quick-frozen in dry ice-ethanol, and stored at −80 °C until use.

Immunofluorescence microscopy

hSAECs were plated on coverslips pretreated with rat tail collagen (Roche). After treatment, cells were fixed with 4 % paraformaldehyde in PBS, permeabilized with 0.1% Triton X-100, blocked and incubated with the primary rabbit polyclonal Abs [49, 50]. After incubation with Alexa-goat anti-rabbit antibody, cells were washed and mounted using ProLong Diamond Antifade Mountant with DAPI (Molecular Probes). The cells were visualized on a Zeiss fluorescence LSM510 confocal microscope using the 63× objective lens.

Subcellular fractionation and Western immunoblot analysis

Sucrose cushion-purified Nuclear proteins were used [49]. For Western blots, equal amounts of protein were resolved by 4–20% SDS-PAGE (Genscript) and transferred to PVDF membranes (Millipore). The membranes were blocked for 1 h at room temperature with Odyssey blocking buffer (LI-COR) and incubated overnight at 4 °C with primary antibodies. After incubation with IRDye 680/800-conjugated secondary antibodies, the membranes were scanned using the Odyssey Infrared Imaging system (LI-COR). The following antibodies were used: IRF1 (sc-497, Santa Cruz), IRF7 (sc-13041, Santa Cruz), ZEB1 (sc-25388, Santa Cruz), ZEB2 (sc-271984, Santa Cruz), α-Tubulin (A01622, Genscript), and LaminB2 (MAB3536, Chemicon).

Microaffinity purification (Biotinylated DNA pulldown) of ISG DNA-binding proteins

A microaffinity DNA pulldown assay for ISG DNA binding proteins was adapted[28, 51]. The natural positive regulatory domain I (PRDI) DNA element from the interferon beta promoter was chemically synthesized with or without 5′ biotin (Bt) labeling (IDT)[29]. The duplex oligonucleotide sequences are listed in Supplementary Table 1. In brief, 50 pmol of biotinylated duplex was incubated with 1 mg of sucrose cushion-purified nuclear protein in 1 ml of binding buffer (8% [vol/vol] glycerol, 5 mM $MgCl_2$, 1 mM dithiothreitol [DTT], 150 mM KCl, 1 mM EDTA, and 12 mM HEPES [pH 7.9]) in the presence of 10 μg of dAdT for 1 h at 4°C. After incubation, bound proteins were captured by adding 50 μL of a 50% slurry of Dynabeads M-280 Streptavidin (Invitrogen) for 20 min at 4°C with mixing. The beads were collected and washed twice with binding buffer. ISG DNA-binding proteins were eluted with 50 μL of 1× SDS-PAGE loading buffer for Western immunoblot analysis. For competition assays, a 10-fold molar excess of the non-biotinylated duplex DNA was added in the initial binding reaction.

Quantitative Real-Time PCR (Q-RT-PCR)

Total RNA was isolated using TRI reagent (Sigma-Aldrich). For gene expression analyses, 5 μg of RNA was reverse transcribed using Super Script III in a 20 μl reaction mixture using gene-specific primers (Supplementary Table 2). The PCR plates were denatured for 3 min at 95°C and then subjected to 40 cycles of 10 s at 95°C, 30 s at 58°C in a CFX96 real-time PCR detection system (Bio-Rad). PCR products were subjected to melting curve analysis to assure that a single amplification product was produced. Quantification of relative changes in mRNA level was determined by the Ct method (normalized to DNA Polymerase beta, *POLB*) and expressed as the fold change between experimental and control samples [52].

Two-step Chromatin Immunoprecipitation (XChIP)

XChIP was performed as described [30]. Briefly, 2–4 ×10^6 hSAECs per 100 mm dish were washed twice with PBS. Protein-protein crosslinking was first performed with Disuccinimidyl glutarate (Pierce), followed by protein-DNA crosslinking with formaldehyde. Equal amounts of sheared chromatin were immuno-precipitated overnight at 4 ℃ with 4 μg of the indicated antibodies in ChIP dilution buffer. Immunoprecipitates were collected with 40 μL Dynabeads Protein-A (Novex), washed, and eluted in 250 μl elution buffer for 15 min at room temperature. Samples were de-crosslinked in 0.2 M NaCl at 65 ℃ for 4 h. The precipitated DNA was phenol/chloroform-extracted, precipitated with 100% ethanol and air-dried. The following antibodies were used: IRF1 (#8478, Cell Signaling), IRF3 (sc-9082, Santa Cruz), IRF7 (sc-13041, Santa Cruz), RelA (sc-372, Santa Cruz), CtBP (sc-11390, Santa Cruz), EZH2 (17–662, Upstate), H3K27me3 (39155, Active Motif), H3K4me3 (ab8580, Abcam), ZEB1 (sc-25388, Santa Cruz) and ZEB2 (sc-271984, Santa Cruz).

Quantitative real-time genomic PCR (Q-gPCR)

Gene enrichment in ChIP was determined by Q-gPCR using region-specific PCR primers and probes (Supplementary Table 3) [30, 53]. The fold change of DNA in each

immunoprecipitate was determined by normalizing the absolute amount to input DNA reference and calculating the fold change relative to the amount in unstimulated cells.

Lentivirus-mediated gene silencing and overexpression

Human *IRF1* and *ZEB*1 cDNAs (gifts from Charles M. Rice [54] and Kumiko UiTei [Addgene plasmid # 42100][55], respectively) were amplified and cloned into the XbaI / EcoRI sites of the lentiviral vector pLV-tetO-CMV-SV40-Puro-LoxP (a gift from George R. Stark [56]) through Gibson assembly. The empty vector was used as a negative control.

TRIPZ inducible lentiviral shRNAs of human *ZEB1* were purchased from Thermo Scientific (V2THS_226625, V2THS_116659 and V2THS_116663). The mature antisense sequences of *ZEB1* shRNAs are listed in Supplementary Table 4. TRIPZ inducible lentiviral non-silencing shRNA (RHS4743) was used as a negative control.

To produce infectious lentivirus, each construct was transfected into 293FT packaging cells together with the lentiviral packaging plasmids using Lipofectamine 2000 (Invitrogen). The supernatant media were collected 48 h after transfection and frozen in aliquots at −80 ℃. hSAECs were infected in the presence of 4 μg/mL polybrene and selected 48 h later with 2 μg/mL of puromycin for 3 d. The stable transfectants from a mixed population were used in the experiments. The lentiviral shRNA stable transfectants were treated with 2 μg/mL of doxycycline (Sigma-Aldrich) for 72 h to induce shRNA-mediated mRNA knockdown.

CRISPR/Cas9-mediated IRF1 gene knockout

The LentiCRISPRv2 system (a gift from Feng Zhang [Addgene plasmid # 52961][57]) was used to prepare lentivirus for *IRF1* gene knockout, with the sgRNA sequence 5'-ACAAGGATGCCTGTTTGTTC –3' targeting exon 3 (Supplementary Figure 7) [58]. The lentiviral CRISPR plasmid targeting human IRF1 was constructed by single-step golden gate sgRNA cloning. hSAECs were infected with virus supernatant in the presence of 4 μg/mL polybrene and selected 48 h later with 2 μg/mL of puromycin for 3 d. 10 d later, the pooled cells were stimulated with 50 μg/mL poly(I:C) for 3 h and analyzed for IRF1 abundance by Western immunoblot. Empty lentiCRISPRv2-transduced hSAECs were puromycin-selected and used as a negative control.

TGFβ-induced pulmonary fibrosis in mice

The design and procedures of animal experiments were approved by the Institutional Animal Care and Use Committee (IACUC) of the University of Texas Medical Branch (Protocol number 1312058). Male C57BL6/J mice aged 16 weeks (The Jackson Laboratory, Bar Harbor, ME) were randomized into two groups (n=5 in each group) and housed under pathogen-free conditions with food and water ad libitum. Mice in treated group were given repetitive challenges with TGFβ (1 μg/mouse intranasally) every other day for a total of 15 TGFβ treatments. Ten days after the last TGFβ treatment, all the mice were sacrificed and lung tissues taken and fixed for immunofluorescence assays blindly.

Statistical analysis

One-way ANOVA was performed when looking for time differences, followed by Tukey's post-hoc test to determine significance. $P<0.05$ was considered significant.

Data availability

The data that support the findings of this study are available from the corresponding authors upon reasonable request. Complete blots for all the figures and corresponding molecular weight markers are shown in Supplementary Figure 12

Supplementary Material

Refer to Web version on PubMed Central for supplementary material.

Acknowledgments

Abbreviations

Ab	antibody
CRISPR/Cas9	clustered regularly interspaced short palindromic repeats / CRISPR associated protein 9
CtBP	C terminal binding protein
EMT	epithelial to mesenchymal transition
EMT-hSAECs	TGFβ-induced mesenchymally transitioned hSAECs
EZH2	Enhancer Of Zeste 2 Polycomb Repressive Complex 2 Subunit
hSAECs	human small airway epithelial cells
PAMPs	pathogen-associated molecular patterns
Q-gPCR	quantitative genomic PCR
Q-RT-PCR	quantitative reverse-transcription PCR
RSV	respiratory syncytial virus
RV16	rhinovirus serotype 16
shRNA	small/ short hairpin RNA
XChIP	dual cross-linked chromatin immunoprecipitation

| **ZEB1** | Zinc Finger E-Box Binding Homeobox 1 |

References

1. To T, et al. Global asthma prevalence in adults: findings from the cross-sectional world health survey. BMC Public Health. 2012; 12:204. [PubMed: 22429515]

2. Lambrecht BN, Hammad H. The airway epithelium in asthma. Nature medicine. 2012; 18:684–692.

3. Holgate ST, et al. Epithelial-mesenchymal communication in the pathogenesis of chronic asthma. Proceedings of the American Thoracic Society. 2004; 1:93–98. [PubMed: 16113419]

4. Saglani S, et al. Early detection of airway wall remodeling and eosinophilic inflammation in preschool wheezers. Am J Respir Crit Care Med. 2007; 176:858–864. [PubMed: 17702968]

5. Johnston SL, et al. Community study of role of viral infections in exacerbations of asthma in 9–11 year old children. BMJ. 1995; 310:1225–1229. [PubMed: 7767192]

6. Johnston NW, Sears MR. Asthma exacerbations. 1: epidemiology. Thorax. 2006; 61:722–728. [PubMed: 16877691]

7. Jamieson KC, Warner SM, Leigh R, Proud D. Rhinovirus in the Pathogenesis and Clinical Course of Asthma. Chest. 2015; 148:1508–1516. [PubMed: 26270739]

8. Liu P, et al. Retinoic acid-inducible gene I mediates early antiviral response and Toll-like receptor 3 expression in respiratory syncytial virus-infected airway epithelial cells. Journal of virology. 2007; 81:1401–1411. [PubMed: 17108032]

9. Slater L, et al. Co-ordinated role of TLR3, RIG-I and MDA5 in the innate response to rhinovirus in bronchial epithelium. PLoS Pathog. 2010; 6:1001178.

10. Fang L, et al. Ataxia telangiectasia mutated kinase mediates NF-kappaB serine 276 phosphorylation and interferon expression via the IRF7-RIG-I amplification loop in paramyxovirus infection. Journal of virology. 2015; 89:2628–2642. [PubMed: 25520509]

11. Tian B, et al. BRD4 Couples NF-kappaB/RelA with Airway Inflammation and the IRF-RIG-I Amplification Loop in Respiratory Syncytial Virus Infection. Journal of virology. 2017; 91

12. de Veer MJ, et al. Functional classification of interferon-stimulated genes identified using microarrays. J Leukoc Biol. 2001; 69:912–920. [PubMed: 11404376]

13. Swider A, Siegel R, Eskdale J, Gallagher G. Regulation of interferon lambda-1 (IFNL1/IFN-lambda1/IL-29) expression in human colon epithelial cells. Cytokine. 2014; 65:17–23. [PubMed: 24140069]

14. Ank N, et al. Lambda interferon (IFN-lambda), a type III IFN, is induced by viruses and IFNs and displays potent antiviral activity against select virus infections in vivo. Journal of virology. 2006; 80:4501–4509. [PubMed: 16611910]

15. Khaitov, MRea. Respiraotry virus induction of alpha-, beta-, and lambda-interferons in bronchial epithelial cells and peripheral blood mononuclear cells. Allergy. 2009; 64:375–386. [PubMed: 19175599]

16. Moore WC, et al. Characterization of the severe asthma phenotype by the National Heart, Lung, and Blood Institute's Severe Asthma Research Program. J Allergy Clin Immunol. 2007; 119:405–413. [PubMed: 17291857]

17. Edwards, MRea. Impaired innate interferon induciton in severee therapy resistant atopic asthmatic children. Mucosal Immunol. 2013; 6:797–806. [PubMed: 23212197]

18. Johnston SL. Innate immunity in the pathogenesis of virus-induced asthma exacerbations. Proceedings of the American Thoracic Society. 2007; 4:267–270. [PubMed: 17607011]

19. Contoli M, et al. Role of deficient type III interferon-lambda production in asthma exacerbations. Nature medicine. 2006; 12:1023–1026.

20. Thomas BJ, et al. Transforming growth factor-beta enhances rhinovirus infection by diminishing early innate responses. Am J Respir Cell Mol Biol. 2009; 41:339–347. [PubMed: 19168696]

21. Mathur SK, et al. Interaction between allergy and innate immunity: model for eosinophil regulation of epithelial cell interferon expression. Ann Allergy Asthma Immunol. 2013; 111:25–31. [PubMed: 23806456]

22. Bedke N, et al. Transforming growth factor-beta promotes rhinovirus replication in bronchial epithelial cells by suppressing the innate immune response. PLoS One. 2012; 7:e44580. [PubMed: 22970254]

23. Kalita M, et al. Systems approaches to modeling chronic mucosal inflammation. Biomed Res Int. 2013; 2013:505864. [PubMed: 24228254]

24. Tian B, et al. Analysis of the TGFbeta-induced program in primary airway epithelial cells shows essential role of NF-kappaB/RelA signaling network in type II epithelial mesenchymal transition. BMC Genomics. 2015; 16:529. [PubMed: 26187636]

25. Ijaz T, et al. Systems biology approaches to understanding Epithelial Mesenchymal Transition (EMT) in mucosal remodeling and signaling in asthma. World Allergy Organ J. 2014; 7:13. [PubMed: 24982697]

26. Zhao Y, Tian B, Sadygov RG, Zhang Y, Brasier AR. Integrative proteomic analysis reveals reprograming tumor necrosis factor signaling in epithelial mesenchymal transition. Journal of proteomics. 2016; 148:126–138. [PubMed: 27461979]

27. Cieslik M, et al. Epigenetic coordination of signaling pathways during the epithelial-mesenchymal transition. Epigenetics Chromatin. 2013; 6:28. [PubMed: 24004852]

28. Jamaluddin M, et al. Angiotensin II induces nuclear factor (NF)-kappaB1 isoforms to bind the angiotensinogen gene acute-phase response element: a stimulus-specific pathway for NF-kappaB activation. Mol Endocrinol. 2000; 14:99–113. [PubMed: 10628750]

29. Escalante CR, Yie J, Thanos D, Aggarwal AK. Structure of IRF-1 with bound DNA reveals determinants of interferon regulation. Nature. 1998; 391:103–106. [PubMed: 9422515]

30. Tian B, Yang J, Brasier AR. Two-step cross-linking for analysis of protein-chromatin interactions. Methods in molecular biology. 2012; 809:105–120. [PubMed: 22113271]

31. Tian B, et al. BRD4 mediates NF-kappaB-dependent epithelial-mesenchymal transition and pulmonary fibrosis via transcriptional elongation. Am J Physiol Lung Cell Mol Physiol. 2016; 311:L1183–L1201. [PubMed: 27793799]

32. Ding S, Robek MD. Peroxisomal MAVS activates IRF1-mediated IFN-lambda production. Nature immunology. 2014; 15:700–701. [PubMed: 25045870]

33. Maniatis T, et al. Structure and function of the interferon-beta enhanceosome. [Review] [59 refs]. Cold Spring Harbor Symposia on Quantitative Biology. 1998; 63:609–620. [PubMed: 10384326]

34. Lu M, Jolly MK, Levine H, Onuchic JN, Ben-Jacob E. MicroRNA-based regulation of epithelial-hybrid-mesenchymal fate determination. Proc Natl Acad Sci U S A. 2013; 110:18144–18149. [PubMed: 24154725]

35. Siegel R, Eskdale J, Gallagher G. Regulation of IFN-lambda1 promoter activity (IFN-lambda1/IL-29) in human airway epithelial cells. J Immunol. 2011; 187:5636–5644. [PubMed: 22058416]

36. Ahn YH, et al. ZEB1 drives prometastatic actin cytoskeletal remodeling by downregulating miR-34a expression. J Clin Invest. 2012; 122:3170–3183. [PubMed: 22850877]

37. Postigo AA, Dean DC. ZEB represses transcription through interaction with the corepressor CtBP. Proc Natl Acad Sci U S A. 1999; 96:6683–6688. [PubMed: 10359772]

38. Zhang Y, et al. Corepressor protein CDYL functions as a molecular bridge between polycomb repressor complex 2 and repressive chromatin mark trimethylated histone lysine 27. J Biol Chem. 2011; 286:42414–42425. [PubMed: 22009739]

39. Zhang Z, et al. PRC2 complexes with JARID2, MTF2, and esPRC2p48 in ES cells to modulate ES cell pluripotency and somatic cell reprogramming. Stem Cells. 2011; 29:229–240. [PubMed: 21732481]

40. McCabe MT, et al. EZH2 inhibition as a therapeutic strategy for lymphoma with EZH2-activating mutations. Nature. 2012; 492:108–112. [PubMed: 23051747]

41. Harada H, et al. Structure and regulation of the human interferon regulatory factor 1 (IRF-1) and IRF-2 genes: implications for a gene network in the interferon system. Mol Cell Biol. 1994; 14:1500–1509. [PubMed: 7507207]

42. Harada H, et al. Absence of the type I IFN system in EC cells: transcriptional activator (IRF-1) and repressor (IRF-2) genes are developmentally regulated. Cell. 1990; 63:303–312. [PubMed: 2208287]

Author Manuscript

43. Wark PA, et al. Asthmatic bronchial epithelial cells have a deficient innate immune response to infection with rhinovirus. The Journal of experimental medicine. 2005; 201:937–947. [PubMed: 15781584]

44. Harris WT, et al. Myofibroblast differentiation and enhanced TGF-B signaling in cystic fibrosis lung disease. PLoS One. 2013; 8:e70196. [PubMed: 23950911]

45. Park JS, et al. Clinical significance of mTOR, ZEB1, ROCK1 expression in lung tissues of pulmonary fibrosis patients. BMC Pulm Med. 2014; 14:168. [PubMed: 25358403]

46. Ramirez RD, et al. Immortalization of human bronchial epithelial cells in the absence of viral oncoproteins. Cancer research. 2004; 64:9027–9034. [PubMed: 15604268]

47. Gern JE. Rhinovirus and the initiation of asthma. Curr Opin Allergy Clin Immunol. 2009; 9:73–78. [PubMed: 19532096]

48. Lee WM, Chen Y, Wang W, Mosser A. Growth of human rhinovirus in H1-HeLa cell suspension culture and purification of virions. Methods in molecular biology. 2015; 1221:49–61. [PubMed: 25261306]

49. Brasier AR, et al. RelA Ser276 phosphorylation-coupled Lys310 acetylation controls transcriptional elongation of inflammatory cytokines in respiratory syncytial virus infection. Journal of virology. 2011; 85:11752–11769. [PubMed: 21900162]

50. Kalita MK, et al. Sources of cell-to-cell variability in canonical nuclear factor-kappaB (NF-kappaB) signaling pathway inferred from single cell dynamic images. J Biol Chem. 2011; 286:37741–37757. [PubMed: 21868381]

51. Brasier AR, et al. A promoter recruitment mechanism for tumor necrosis factor-alpha-induced interleukin-8 transcription in type II pulmonary epithelial cell. Dependence on nuclear abundance of Rel A, NF-kappaB1, and c-Rel transcription factors. J Biol Chem. 1998; 273:3551–3561. [PubMed: 9452482]

52. Yang J, et al. Systematic Determination of Human Cyclin Dependent Kinase (CDK)-9 Interactome Identifies Novel Functions in RNA Splicing Mediated by the DEAD Box (DDX)-5/17 RNA Helicases. Molecular & cellular proteomics : MCP. 2015; 14:2701–2721. [PubMed: 26209609]

53. Yang J, et al. A probabilistic approach to learn chromatin architecture and accurate inference of the NF-kappaB/RelA regulatory network using ChIP-Seq. Nucleic Acids Res. 2013; 41:7240–7259. [PubMed: 23771139]

54. Schoggins JW, et al. Pan-viral specificity of IFN-induced genes reveals new roles for cGAS in innate immunity. Nature. 2014; 505:691–695. [PubMed: 24284630]

55. Mazda M, Nishi K, Naito Y, Ui-Tei K. E-cadherin is transcriptionally activated via suppression of ZEB1 transcriptional repressor by small RNA-mediated gene silencing. PLoS One. 2011; 6:e28688. [PubMed: 22205962]

56. Cheon H, et al. IFNbeta-dependent increases in STAT1, STAT2, and IRF9 mediate resistance to viruses and DNA damage. EMBO J. 2013; 32:2751–2763. [PubMed: 24065129]

57. Sanjana NE, Shalem O, Zhang F. Improved vectors and genome-wide libraries for CRISPR screening. Nat Methods. 2014; 11:783–784. [PubMed: 25075903]

58. Shalem O, et al. Genome-scale CRISPR-Cas9 knockout screening in human cells. Science. 2014; 343:84–87. [PubMed: 24336571]
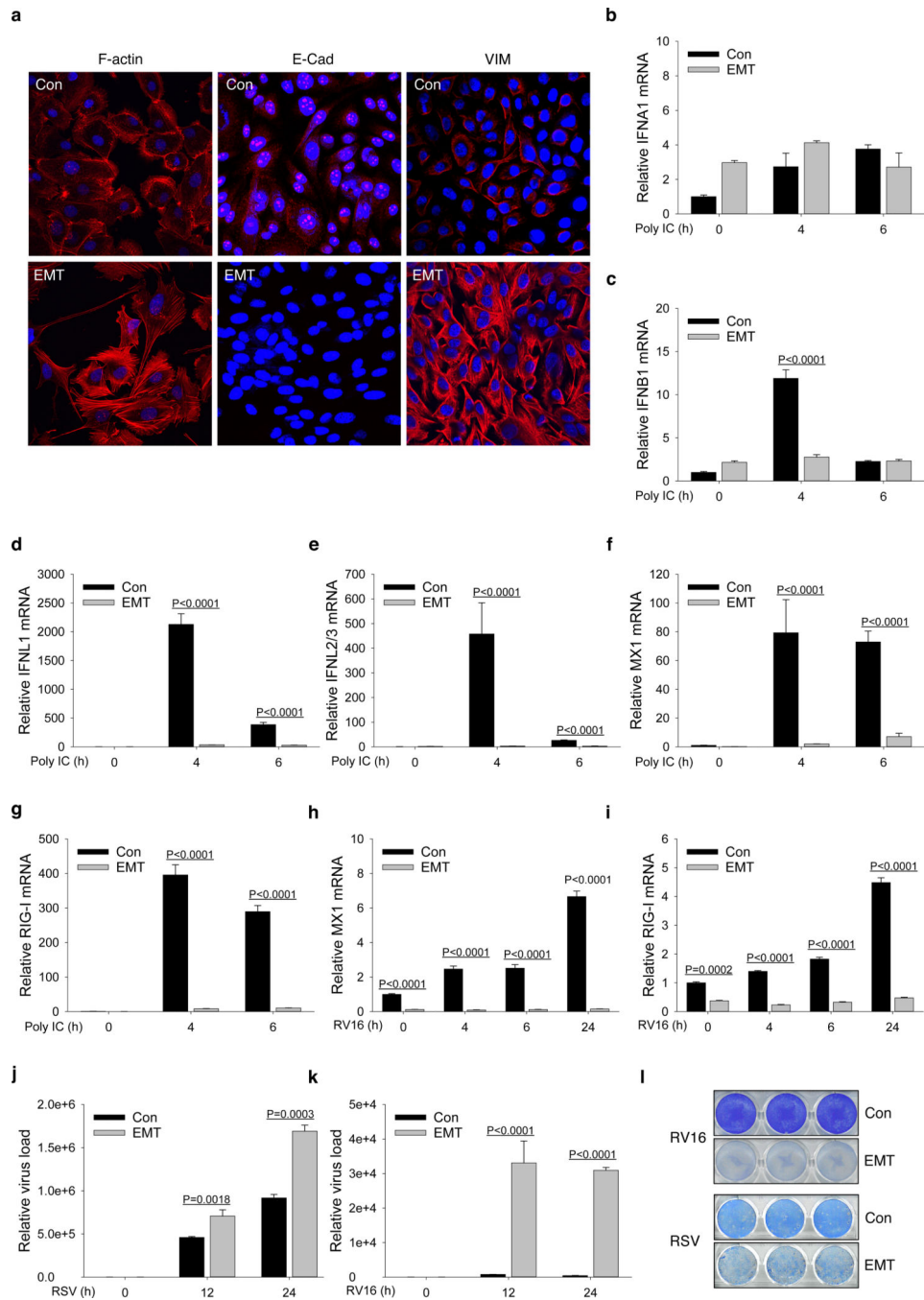
Figure 1. Deficient type I/III IFN responses in TGFβ-induced EMT

a, Confocal immunofluorescence imaging of hSAECs (Con) and EMT-hSAECs (EMT, induced by 10 ng/mL TGFβ treatment for 15 days). Distribution of F-actin, E-Cadherin (E-Cad) and vimentin (VIM) was shown by staining with Alexa 568-conjugated phalloidin or secondary antibody (red); nuclei were counterstained with DAPI (blue). Shown is the representative staining from five images. **b – g**, Q-RT-PCR analysis of: type I interferons *IFNA1* (**b**) and *IFNB1* (**c**), type III interferons *IFNL1* (**d**) and *IFNL2/3* (**e**), and interferon-stimulated genes (ISGs) *MX1* (**f**) and *RIG-I* (**g**) in hSAECs (Con) and EMT-hSAECs

(EMT), stimulated by poly IC (50 μg/mL) for 0h, 4h and 6h. The results were quantified relative to the signal of DNA polymerase beta (*POLB*) and shown as fold-change of mRNA abundance normalized to unstimulated samples (Con). **h – i**, Q-RT-PCR analysis of the interferon-stimulated genes (ISGs) *MX1* (**h**) and *RIG-I* (**i**) in hSAECs (Con) and EMT-hSAECs (EMT) infected by RV16 for 0h, 4h, 6h and 24h. **j – k**, Q-RT-PCR analysis of relative virus load in hSAECs (Con) and EMT-hSAECs (EMT), infected by RSV (**j**) or RV16 (**k**) for 0h, 12h and 24h. The results are shown as fold changes of RV16 viral RNA 5' UTR and RSV N viral RNA, respectively. Data are the means ± S.D. from n=3 biological replicates. **l**, Virus plaque assays of hSAECs (Con) and EMT-hSAECs (EMT) infected by RSV or RV16 for 24h (MOI = 1). Virus plaques were detected in triplicate in HEp-2 (RSV) or H1HeLa cells (RV16), using serial 2-fold dilutions of cell culture supernatants or freeze-thawed cellular lysates, respectively. Plaques were stained at 5 days (RSV) or 9 days (RV16) post-infection. Shown are the representative triplicates at the same dilution. The complete view of these virus plaque data can be seen in Supplementary Figure 1.
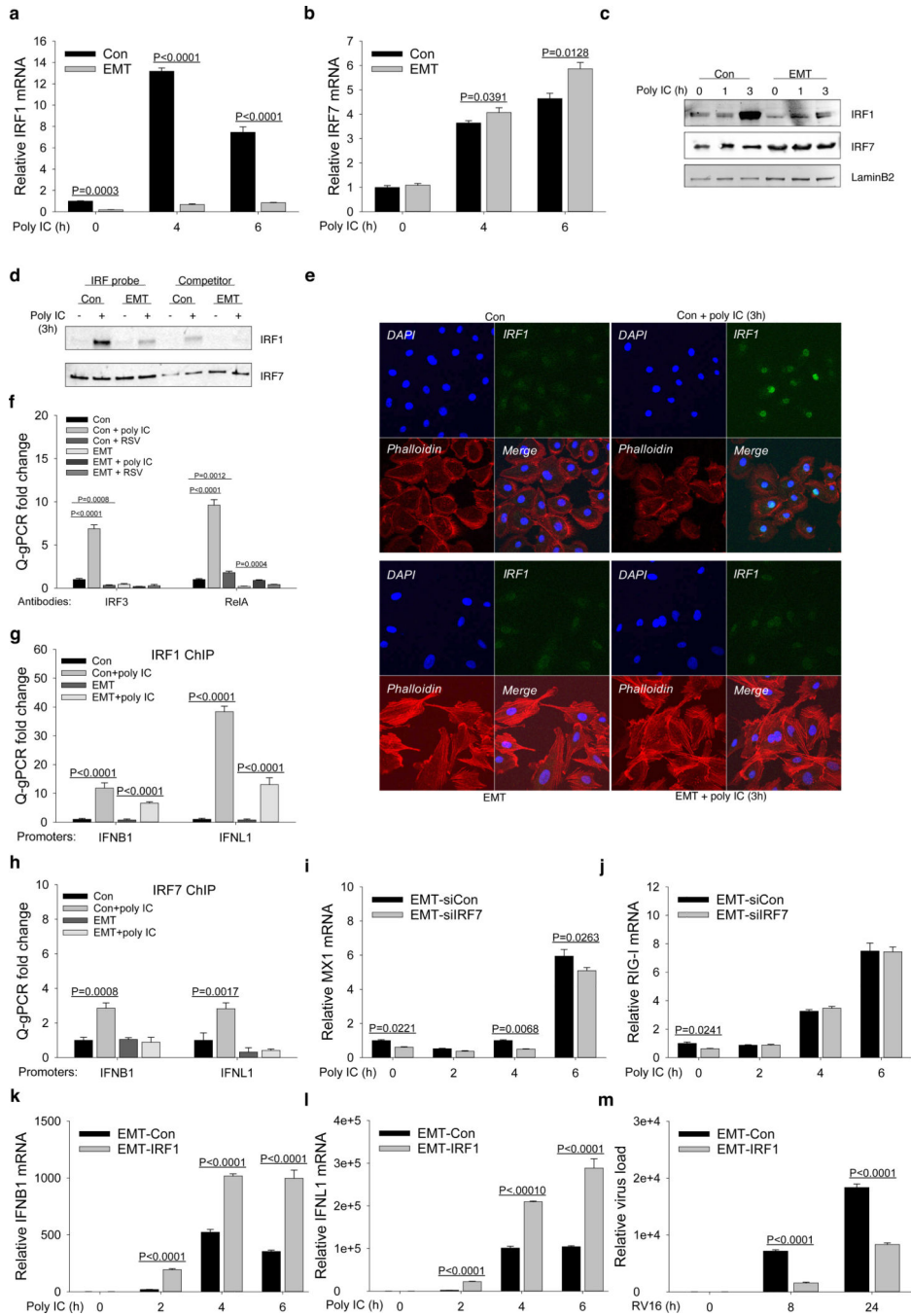
Figure 2. IRF1 silencing dysregulates the IFN response in TGFβ-induced EMT

a – b, Q-RT-PCR analysis of *IRF1* (**a**) and *IRF7* (**b**) in hSAECs (Con) and EMT-hSAECs (EMT), stimulated with 50 μg/mL poly(I:C) for 0h, 4h and 6h. **c**, Western blot analysis of IRF1 and IRF7 in cellular nuclear fractions of hSAECs (Con) and EMT-hSAECs (EMT) stimulated with 50 μg/mL poly(I:C) for 0h, 1h and 3h. LaminB2 was used as a loading control. Shown are representative blots from three experiments. **d**, Microaffinity capture of poly(I:C)-inducible ISG/DNA-binding proteins. Nuclear extracts from hSAECs (Con) and EMT-hSAECs (EMT) in the absence or presence of poly(I:C) stimulation (50 μg/mL for 3h)

were affinity-purified by biotinylated ISG duplex DNA or non-biotinylated competitor, captured by streptavidin beads and probed with the indicated Abs on Western blots. Shown are representative blots from two experiments. **e**, Confocal immunofluorescence imaging for IRF1 in hSAECs (Con) or EMT-hSAECs (EMT) stimulated with 50 μg/mL poly(I:C) for 3h. The secondary Ab was Alex Fluo 488 (green). Shown is the representative staining from five images. **f**, XChIP assay for IRF3 and RelA binding to the *IRF1* promoter in hSAECs (Con) or EMT-hSAECs (EMT) stimulated with 50 μg/mL poly(I:C) for 3 h or infected with RSV at MOI 0.5 for 15 h. Data were quantified relative to the input signal and shown as fold-change normalized to unstimulated samples (Con). **g**, XChIP assay of IRF1 binding to the *IFNB1* and *IFNL1* promoters in hSAECs (Con) or EMT-hSAECs (EMT) stimulated with 50 μg/mL poly(I:C) for 3h. **h**, XChIP assay of IRF7 binding to *IFNB1* and *IFNL1* promoters in hSAECs (Con) or EMT-hSAECs (EMT) stimulated with 50 μg/mL (polyI:C) for 3h. **i-j**, Q-RT-PCR analysis of *MX1* (**i**) and *RIG-I* (**j**) in control siRNA (EMT-siCon)- or *IRF7* siRNA (EMT-siIRF7)- transfected EMT-hSAECs, stimulated with 50 μg/mL poly(I:C) for 0h, 2h, 4h and 6h. **k – l**, Q-RT-PCR analysis of *IFNB1* (**k**) and *IFNL1* (**l**) in lentiviral IRF1 stably transduced EMT-hSAECs (EMT-IRF1) stimulated with 50 μg/mL poly(I:C) for 0 h, 2 h, 4 h and 6 h. The empty lentiviral-transduced EMT-hSAECs were used as controls (EMT-Con). **m**, Q-RT-PCR analysis of RV16 viral RNA 5' UTR in EMT-Con and EMT-IRF1 cells infected with RV16 (MOI = 1) for 0 h, 8 h and 24 h. Data are the mean ± S.D. from n=3 biological replicates.
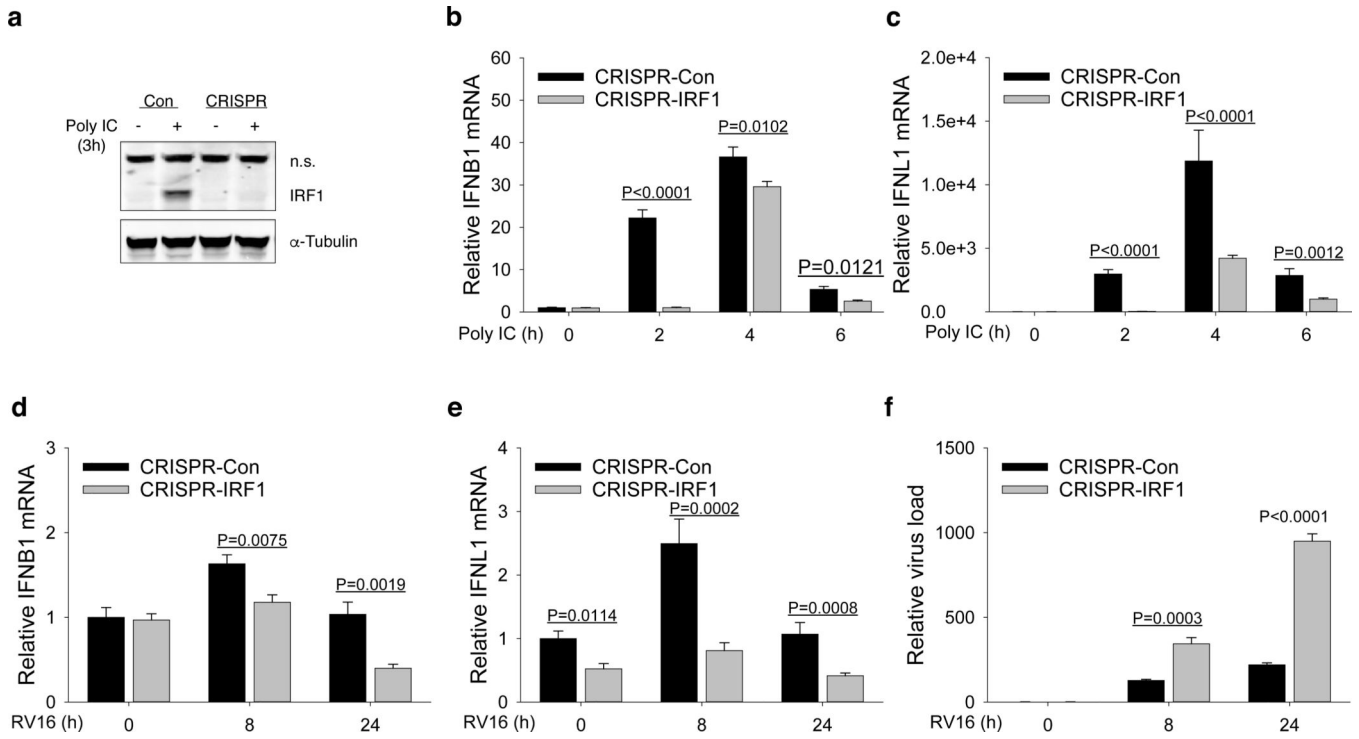
Figure 3. CRISPR/Cas9-mediated IRF1 gene knockout
a, Western blot analysis of CRISPR/Cas9-mediated IRF1 knockout. hSAECs stably transduced by empty lentiCRISPR (Con) or lentiCRISPRv2 with *IRF1* sgRNA (CRISPR) were stimulated with 50 μg/mL poly(I:C) for 0h (−) and 3h (+). Total cell lysates were detected using IRF1 Ab. α-Tubulin blot is shown as the loading control. Shown are representative blots from two experiments. **b – c**, Q-RT-PCR analysis of *IFNB1* (**b**) and *IFNL1* (**c**) in cells used in **a** and stimulated with 50 μg/mL poly(I:C) for 0h, 2h, 4h and 6h. **d – f**, Q-RT-PCR analysis of *IFNB1* (**d**), *IFNL1* (**e**) and RV16 viral RNA 5' UTR (**f**) in cells used in **a** and infected with RV16 for 0h, 8h and 24h. Data are the mean ± S.D. from n=3 biological replicates.
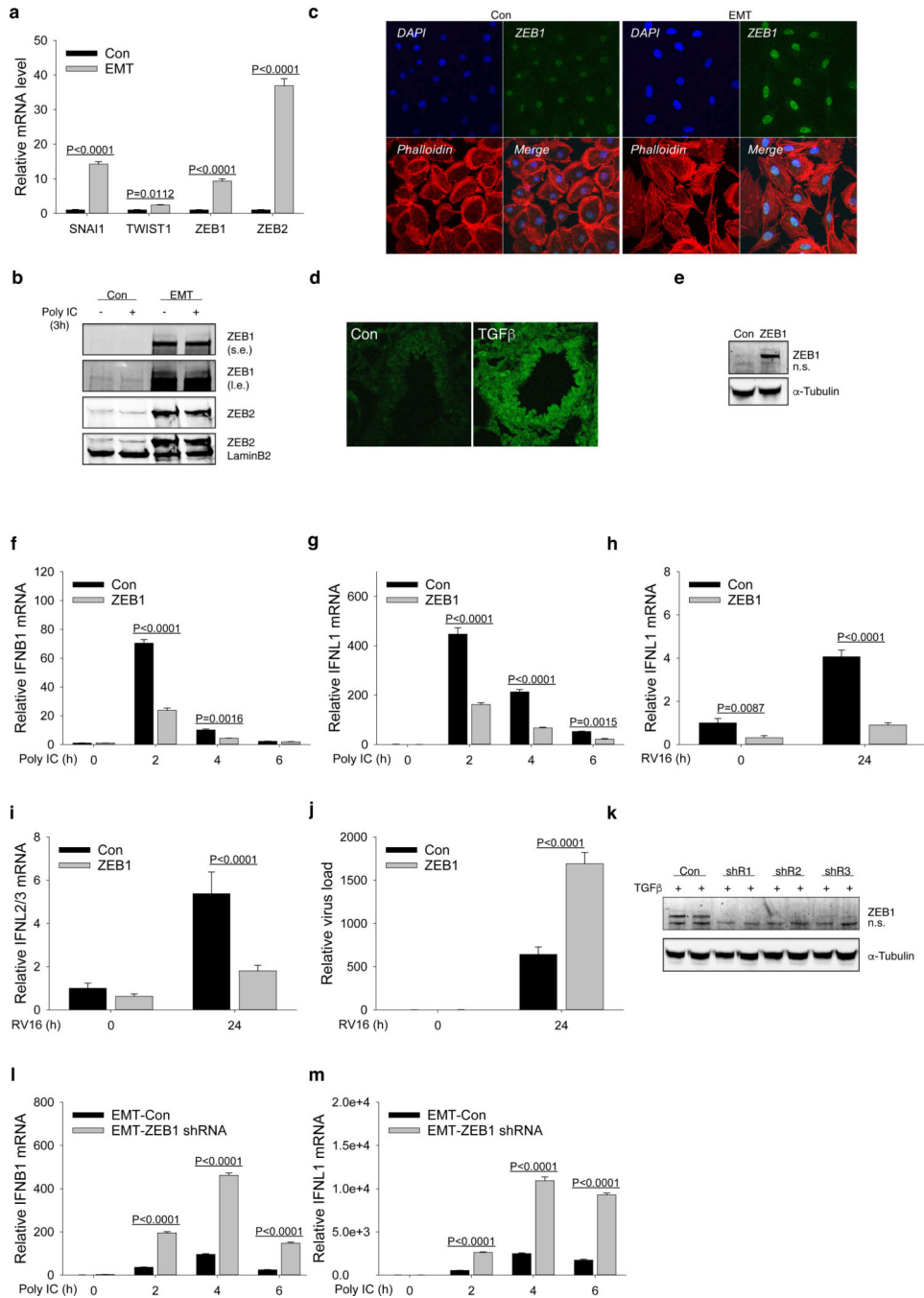
Figure 4. ZEB1 downregulates the IFN response in hSAECs and TGFβ-induced EMT-hSAECs
a, Q-RT-PCR analysis of EMT core transcription factors (*SNAIL1 TWIST1 ZEB1* and *ZEB2*) in hSAECs (Con) and EMT-hSAECs (EMT). **b**, Western blot analysis of ZEB1 and ZEB2, using cellular nuclear exacts from hSAECs (Con) and EMT-hSAECS (EMT) stimulated with 50 μg/mL poly(I:C) for 0h and 3h. LaminB2 was used as the loading control. s.e., short exposure; l.e., long exposure. **c**, Confocal immunofluorescence imaging for ZEB1 in hSAECs (Con) or EMT-hSAECs (EMT). The secondary Ab was Alex Fluo 488 (green). **d**, Confocal immunofluorescence staining of ZEB1 in mouse lung from chronic

TGFβ-induced fibrosis/EMT. Con, PBS-treated mouse lung; TGFβ, TGFβ—treated mouse lung. Shown is the representative staining from five images. **e**, Western blot analysis of ZEB1, and α-tubulin as loading control, using total protein exacts from hSAECs stably transduced with Lentiviral ZEB1. The empty lentiviral-transduced hSAECs were used as controls. Shown are representative blots from two experiments. n.s, nonspecific bands. **f – g**, Q-RT-PCR analysis of *IFNB1* (**f**) and *IFNL1* (**g**) in Con and ZEB1 cells used in **c**, stimulated with 50 μg/mL poly(I:C) for 0h, 2h, 4h and 6h. **h-j**, Q-RT-PCR analysis of *IFNL1* (**h**), *IFNL2*/*3* (**i**) and RV16 viral RNA 5' UTR (**j**) in Con and ZEB1 cells used in **c**, infected with RV16 (MOI = 1) for 24h. Data are shown as fold change normalized to unstimulated cells (Con). **k**, Western blot analysis of ZEB1, and α-tubulin as loading control, using total protein exacts from hSAECs stably transduced with 3 inducible lentiviral *ZEB1* shRNAs (shR1, shR2 and shR3). Cells were first induced to EMT by 10 ng/mL of TGFβ for 15 days and then treated with 2 μg/mL doxycycline for 72 h. Cellular samples were treated and collected in biological duplicates. Non-silencing shRNA-transduced cells under the same conditions were used as controls (EMT-Con). Shown are representative blots from two experiments. **l – m** , Q-RT-PCR analysis of *IFNB1* (**l**) and *IFNL1* (**m**) in *ZEB1* shRNA (shR1)-depleted EMT-hSAECs (same treatment as in **k**) stimulated with 50 μg/mL poly(I:C) for 0h, 2h, 4h and 6h. Data are the mean ± S.D. from n=3 biological replicates.
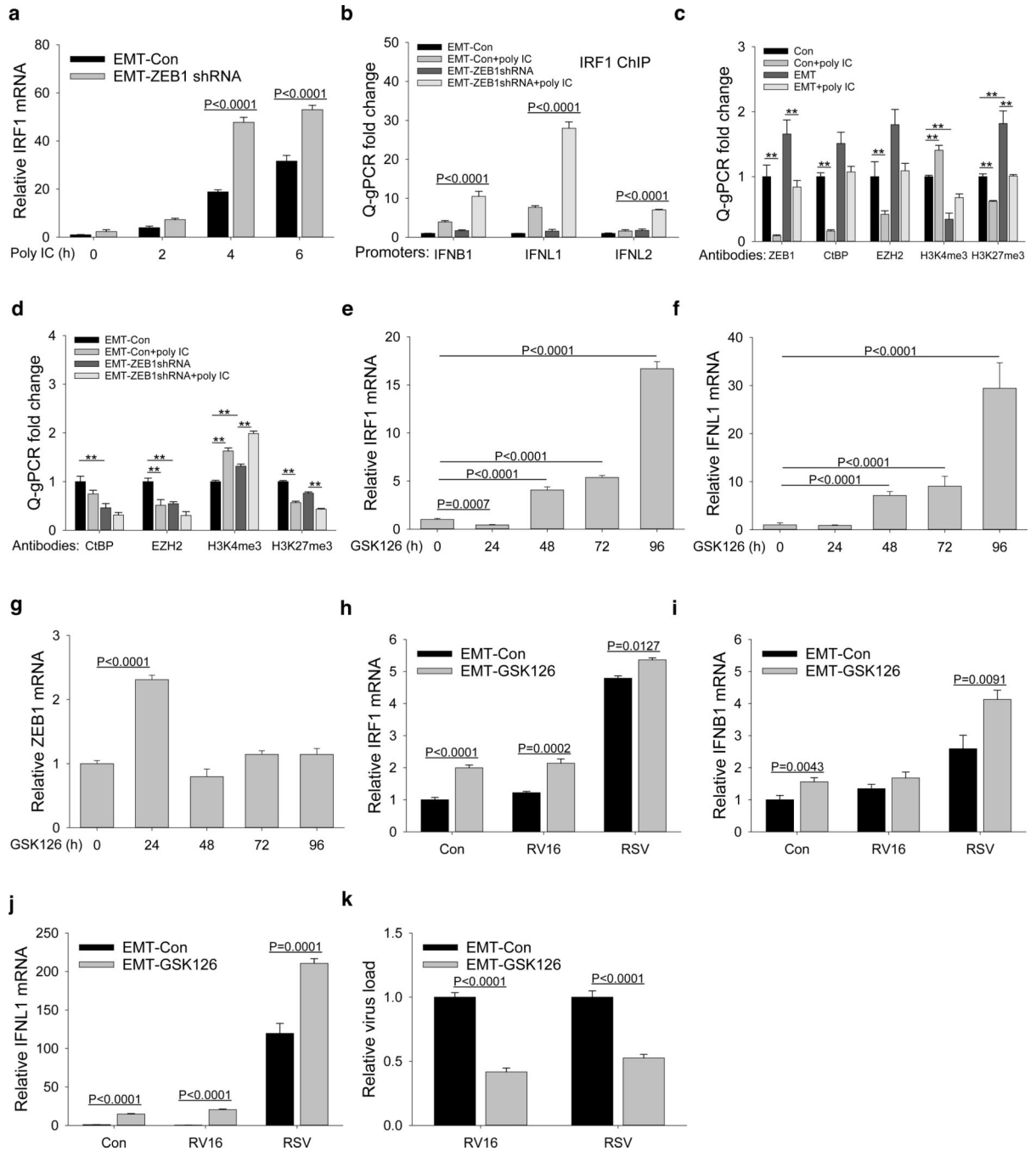
Figure 5. ZEB1 downregulates the IFN response via epigenetic silencing of IRF1

a, Q-RT-PCR analysis of *IRF1* in ZEB1 shRNA (shR1)-depleted EMT-hSAECs stimulated with 50 μg/mL poly(I:C) for 0h, 2h, 4h and 6h (under the same experimental conditions as in Figure 4 **l-m**). **b**, XChIP assay of IRF1 in cells used in panel **a** and stimulated with 50 μg/mL poly(I:C) for 3h. Chromatin was cross-linked and immunoprecipitated with anti-IRF1 Ab. Shown is probe-based Q-gPCR analysis of specific promoters for *IFNB1 IFNL1* and *IFNL2*. Data were quantified relative to the signal of input and shown as fold change normalized to non-silencing shRNA control (EMT-Con). ******, P < 0.0001. **c**, XChIP assay in

hSAECs (Con) or EMT-hSAECs (EMT) stimulated with 50 μg/mL poly(I:C) for 3h. Chromatin was cross-linked and immunoprecipitated with Abs for ZEB1, CtBP, EZH2, H3K4me3 and H3K27me3, respectively. Shown is probe-based Q-gPCR analysis of the *IRF1* promoter region. **, P < 0.0001. **d**, XChIP assay of CtBP, EZH2, H3K4me3 and H3K27me3 in cells used in panel **a** and stimulated with 50 μg/mL poly(I:C) for 3h. Chromatin was cross-linked and immunoprecipitated with Abs for CtBP, EZH2, H3K4me3 and H3K27me3. Shown is probe-based Q-gPCR analysis for the *IRF1* promoter. Data were quantified relative to the signal of input and shown as fold change normalized to shRNA control (EMT-Con). **, P < 0.0001. **e – g**, Q-RT-PCR analysis of *IRF1* (**e**), *IFNL1* (**f**) and *ZEB1* (**g**) in EMT-hSAECs treated with the specific EZH2 methyltransferase inhibitor GSK126 for a time series of 0 h, 24 h, 48 h, 72 h and 96 h. Data are expressed as fold change relative to solvent-treated cells (0 h). **h-k**, Q-RT-PCR analysis of *IRF1* (**h**), *IFNB1* (**i**), *IFNL1* (**j**), RSV N viral RNA and RV16 viral RNA 5' UTR (**k**) in EMT-hSAECs pretreated with the specific EZH2 methyltransferase inhibitor GSK126 for 72h, followed by infection with RV16 or RSV (MOI = 1) for 24h. Data are shown as fold change normalized to unstimulated cells (Con). Data are the means ± S.D. from n=3 biological replicates.
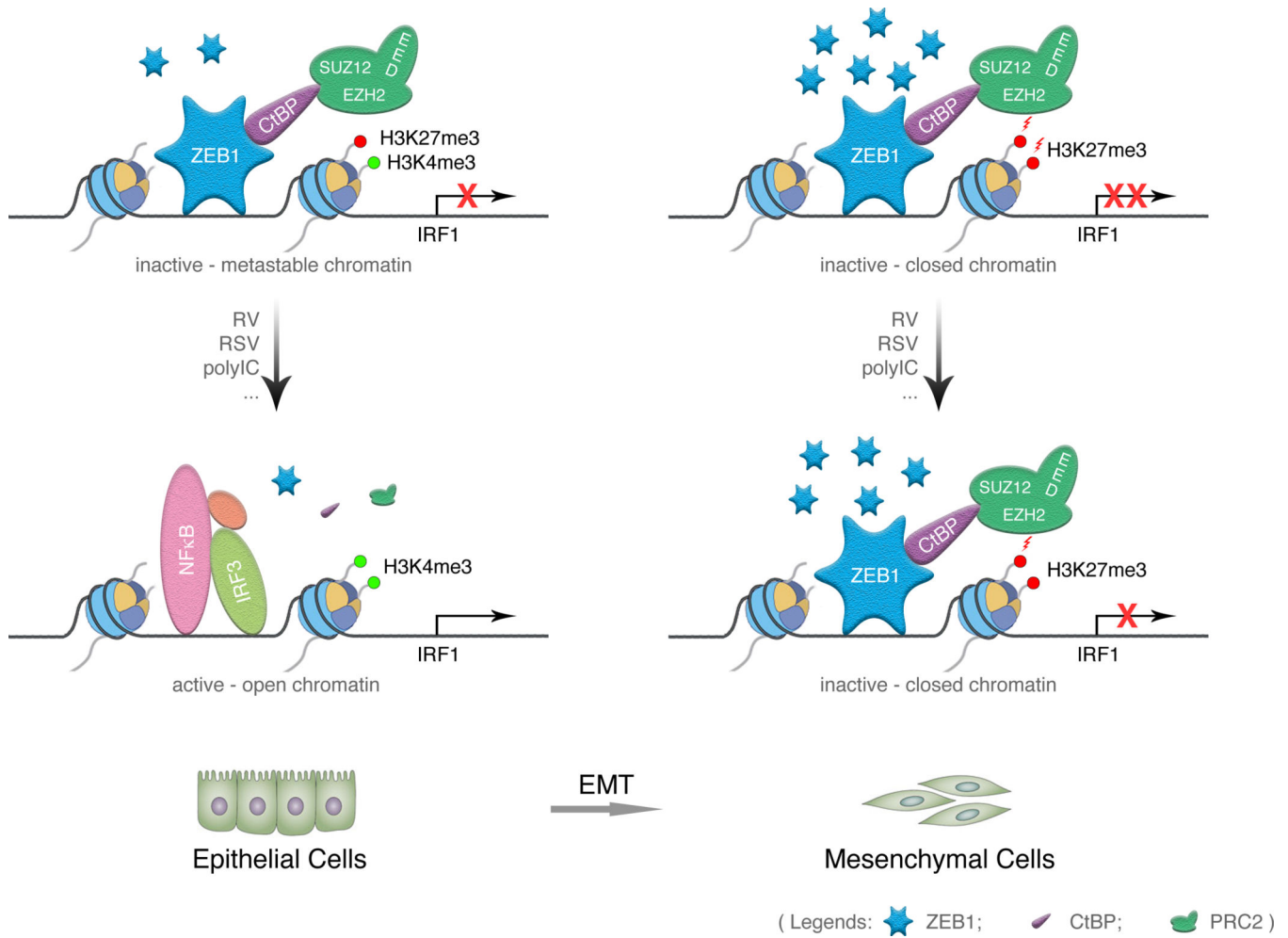
Figure 6. ZEB1-mediated epigenetic regulation of IRF1

Schematic model of the *IRF1* promoter in epithelial cells (left) and mesenchymal cells (right). In unstimulated epithelial cells, *IRF1* is in a metastable state associated with activating histone H3 K4(me3) and suppressive histone H3 K27 (me3) marks, controlled by the ZEB1-CtBP complex. Upon activation by viral patterns, ZEB1-CtBP is cleared from the promoter, associated with recruitment of activating NFκB and IRF3. By contrast, in the mesenchymal transition, upregulated ZEB1-CtBP replaces the activating histone marks with H3K27(me3) mediated by EZH2, functionally repressing the promoter and downstream expression of IFN-III.